Supporting Information for: Transferable Anisotropic United-Atom Mie (TAMie) Force-Field: Transport properties from Equilibrium Molecular Dynamic Simulations

Matthias Fischer, Gernot Bauer, and Joachim Gross*

Institute of Thermodynamics and Thermal Process Engineering, University of Stuttgart, Pfaffenwaldring 9, 70569 Stuttgart

E-mail: gross@itt.uni-stuttgart.de

Phone: +49 (0)711 685 66103. Fax: +49 (0)711 685 66140

SAFT Parameters used in this Study

Table S1: PC-SAFT Parameters used for the substances in this study

CAS	Substance	Molar Weight / $\mathrm{g\,mol^{-1}}$	m	σ / Å	ϵ/k/K	κ_{ab}	ϵ_{ab}/k/K	DM/D
74840	ethane	30.07	1.6069	3.5206	191.42	0	0	0
74986	propane	44.096	2.002	3.6184	208.11	0	0	0
110543	hexane	86.177	3.0576	3.7983	236.77	0	0	0
111842	nonane	128.25	4.2079	3.8448	244.51	0	0	0
106989	1-butene	56.107	2.2864	3.6431	222	0	0	0
592767	1-heptene	98.1861	3.2863	3.8138	243.756	0	0	0.6296
115106	dimethylether	46.069	2.2634	3.2723	210.29	0	0	1.3
75070	ethanal	44.0526	2.1188	3.246	229.851	0	0	2.6891
123728	butanal	72.107	2.8825	3.4698	247.09	0	0	2.72
111717	heptanal	114.185	3.8527	3.66	260.698	0	0	2.5782
67641	acetone	58.08	2.7447	3.2742	232.99	0	0	2.88
78933	butanone	72.107	2.9835	3.4239	244.99	0	0	2.78

Parameters of the TAMie force field

Tables S2 to S5 provide the parameters of the TAMie force field as described in the *Molecular Model* section in the main text. The parameters were all published in previous work[1–3,3], except for the bond constant k_l in Table S3, which was specified by the authors of this study.

Table S2: Pair potential parameters of UA-groups used in this study: Energy parameter ε_{ii}, size parameter σ_{ii}, repulsive exponent n_{ii}, and point charge q_i for the TAMie force field

United atom i	$M_{ii}/(\mathrm{g\,mol^{-1}})$	$\varepsilon_{ii}/k_\mathrm{B}/\mathrm{K}$	$\sigma_{ii}/\mathrm{Å}$	n_{ii}	q_i/e
CH_3	15.035	136.318	3.6034	14	0.175 (next to ether O)
CH_3 (ethane)	15.035	130.780	3.6463	14	—
CH_2	14.027	52.913	4.0400	14	—
CH_2 (olefins)	14.027	100.681	3.6005	14	—
CH (olefins)	13.019	53.951	3.8234	14	—
O (dimethyl ether)	15.999	54.36	3.213	12	−0.35
O (aldehydes)	15.999	100.58	3.0276	12	−0.422
CH_x (neighbor ald.)					−0.038
CH (aldehydes)	13.019	68.934	3.4941	12	0.46
O (ketones)	15.999	65.55	3.093	12	−0.49
C (ketones)	12.011	32.775	3.919	12	0.49
O (acetone)	15.999	69.184	3.112	12	−0.49
C (acetone)	12.011	34.592	3.942	12	0.49

Table S3: Bond lengths and constants of the TAMie force field used in this study ($x, y \in \{1, 2\}$)

Bond	$r_0/\mathrm{Å}$	$k_l/\mathrm{K\,Å^{-2}}$
CH_3−CH_3 (ethane)	1.94	100 644
CH_3−CH_x	1.74	100 644
CH_x−CH_y	1.54	100 644
CH=CH_x	1.33	100 644
CH_3−CH[=O_{ald}]	1.74	100 644
CH_2−CH[=O_{ald}]	1.54	100 644
CH=O_{ald}	1.217	100 644
CH_3−C[=O_{ket}]	1.74	100 644
CH_2−C[=O_{ket}]	1.54	100 644
C=O_{ket}	1.229	100 644
CH_3−O_{ether}	1.61	100 644

Table S4: Bending angles and constants of the TAMie force field used in this study ($x, y \in \{2, 3\}$ and $z \in \{1, 2\}$)

Bending sites	θ_0/deg	k_θ/k_B/K
$\mathrm{CH}_x\mathrm{-CH_2-CH}_y$	114.0	62 500
$\mathrm{CH}_z\mathrm{=CH-CH}_y$	119.7	70 420
$\mathrm{CH}_x\mathrm{-O}_\mathrm{ether}\mathrm{-CH}_y$	112.0	60 400
$\mathrm{CH}_x\mathrm{-C}_\mathrm{ket}\mathrm{-CH}_y$	117.2	62 500
$\mathrm{C}_\mathrm{ket}\mathrm{-CH_2-CH}_x$	114.0	62 500
$\mathrm{CH}_x\mathrm{-C}_\mathrm{ket}\mathrm{=O}_\mathrm{ket}$	121.4	62 500
$\mathrm{CH}_x\mathrm{-CH=O}_\mathrm{ald}$	121.4	62 500

Table S5: Torsion potential constants of the TAMie force field used in this study ($x, y \in \{2, 3\}$ and $z \in \{1, 2\}$)

Torsion sites	c_0/k_B/K	c_1/k_B/K	c_2/k_B/K	c_3/k_B/K
$\mathrm{CH}_x\mathrm{-CH_2-CH_2-CH}_y$	0.0	355.03	−68.19	791.32
$\mathrm{CH}_x\mathrm{-CH_2-O}_\mathrm{ether}\mathrm{-CH}_y$	0.0	725.35	−163.75	558.2
$\mathrm{CH}_x\mathrm{-CH_2-CH_2-CH}_y$	0.0	176.62	−53.34	769.93
$\mathrm{CH}_z\mathrm{=CH-CH_2-CH}_y$	688.5	86.36	−109.77	−282.24
$\mathrm{C-CH_2-CH_2-CH}_y$	0.0	355.03	−68.19	791.32
$\mathrm{CH}_x\mathrm{-CH_2-C=O}_\mathrm{ket}$	2035.58	−736.90	57.84	−293.23
$\mathrm{CH}_x\mathrm{-C-CH_2-CH}_y$	−17.26	752.60	14.89	282.10
$\mathrm{CH}_x\mathrm{-CH_2-CH_2-CH[=O}_\mathrm{ald}\mathrm{]}$	11.81	467.80	−274.10	846.80
$\mathrm{CH}_x\mathrm{-CH_2-CH=O}_\mathrm{ald}$	1182.0	−225.60	302.20	−339.30

Correlation Parameters from Simulation

Tables S6 to S8 summarize the parameters of the entropy correlations for each transport property adjusted to the simulation results. The corresponding correlation functions can be found in Table 3 in the main text. Additional to the parameters, the AAD of each correlation to all available experiments is given for each substance, along with the number of experimental data points available. The sources of the experiments are given in the column *Lit.*

Table S6: Entropy Scaling Parameters of the TAMie force field for viscosity

CAS	Substance	A_η	B_η	C_η	D_η	$N_{\text{exp.}}$	$AAD_{\text{exp.}}$	Lit.
74840	ethane	−0.584 82	−1.597	−0.119 57	−0.015 513	2606	5.93 %	[4]
74986	propane	−0.739 04	−1.9377	−0.317 13	−0.051 261	1752	9.47 %	[4]
110543	hexane	−1.3007	−2.6303	−0.508 42	−0.090 849	1804	9.90 %	[4]
111842	nonane	−1.5238	−3.0059	−0.638 05	−0.136 35	382	14.45 %	[4]
106989	1-butene	−0.8661	−2.207	−0.440 46	−0.071 512	22	5.59 %	[4]
592767	1-heptene	−1.1781	−2.5061	−0.489 27	−0.101 39	163	6.79 %	[4]
115106	dimethylether	−0.8927	−2.0926	−0.375 23	−0.070 398	211	6.31 %	[4]
75070	ethanal	−0.978 54	−1.8377	−0.2819	−0.072 213	28	11.61 %	[4]
123728	butanal	−1.084	−2.388	−0.556 46	−0.132 42	233	15.12 %	[4]
111717	heptanal	−1.4179	−2.843	−0.551 04	−0.133 02	12	30.16 %	[4]
67641	acetone	−1.1162	−2.3125	−0.535 79	−0.147 13	512	15.28 %	[4]
78933	butanone	−1.2108	−2.4107	−0.471 33	−0.123 34	246	22.00 %	[4]

Table S7: Entropy Scaling Parameters of the TAMie force field for thermal conductivity

CAS	Substance	A_λ	B_λ	C_λ	D_λ	$N_{\text{exp.}}$	$AAD_{\text{exp.}}$	Lit.
74840	ethane	−0.416 97	−1.3177	0.538 18	−0.120 65	1629	16.43 %	[4]
74986	propane	−0.3735	−0.745 96	1.2519	−0.027 495	3154	13.35 %	[4]
110543	hexane	−0.128 34	−0.835 16	1.0578	−0.077 646	646	11.23 %	[4]
111842	nonane	−0.043 518	−0.380 23	1.7543	0.031 92	524	6.00 %	[4]
106989	1-butene	−0.127 92	−1.06	0.443 67	−0.075 675	31	11.03 %	[4]
592767	1-heptene	−0.063 358	−0.650 59	1.226	−0.033 603	415	7.69 %	[4]
115106	dimethylether	−0.528 64	−0.732 68	1.4949	−0.026 342	347	15.94 %	[4]
75070	ethanal	−0.549 35	−1.1198	0.824 21	−0.078 127	96	11.57 %	[4]
123728	butanal	−0.247 26	0.187 17	2.4271	0.124 88	82	10.35 %	[4]
111717	heptanal	−0.162	0.307 38	2.7413	0.144 91	12	1.98 %	[4]
67641	acetone	−0.568 02	−0.7099	1.3292	−0.001 708 6	386	9.44 %	[4]
78933	butanone	−0.422 98	−0.132 37	2.0665	0.0883	347	7.99 %	[4]

Table S8: Entropy Scaling Parameters of the TAMie force field for diffusion

CAS	Substance	$A_{D_{\text{self}}}$	$B_{D_{\text{self}}}$	$C_{D_{\text{self}}}$	$N_{\text{exp.}}$	$AAD_{\text{exp.}}$	Lit.
74840	ethane	−0.373 69	0.148 59	2.4814×10^{-13}	154	14.40 %	[5–9]
74986	propane	−0.536 49	0.159 84	9.9011×10^{-15}	75	20.66 %	[7,9]
110543	hexane	−0.707 72	0.268 65	4.8284×10^{-14}	185	21.16 %	[8–15]
111842	nonane	−0.909 91	0.392 24	7.1876×10^{-13}	104	18.72 %	[9,10,15–17]
106989	1-butene	−0.682 83	0.142 48	8.2794×10^{-3}	0	–	–
592767	1-heptene	−0.790 56	0.283 69	1.9320×10^{-14}	0	–	–
115106	dimethylether	−0.553 05	0.203 44	3.0468×10^{-13}	40	7.98 %	[9]
75070	ethanal	−0.4574	0.227 17	1.3107×10^{-13}	0	–	–
123728	butanal	−0.6685	0.300 23	7.3716×10^{-14}	0	–	–
111717	heptanal	−0.853 65	0.433 13	1.3380×10^{-13}	0	–	–
67641	acetone	−0.668 09	0.319 03	1.6004×10^{-13}	48	24.86 %	[9]
78933	butanone	−0.694 77	0.335 19	1.0136×10^{-13}	0	–	–

Simulation Results of each Substance

This section contains tables summarizing temperatures T, pressures p, reduced entropies s^*, viscosities η, self-diffusion coefficients D_{self}, and thermal conductivities λ for all investigated substances. The first part of each table describes the simulated state points with the corresponding reduced entropy, calculated using PC-SAFT. The second part provides the simulation results for the transport properties. The respective state points can be assigned via s^*.

Table S9: Results of ethane

ρ/kg/m^3	T/K	p/bar	s^*
598.62	135.55(4)	8.4677(130000)	−3.3338
540.97	184.27(3)	7.9153(82000)	−2.4914
450.66	247.380(47)	11.396(4200)	−1.6576
308.42	310.470(61)	61.119(1100)	−0.912 27
16.067	246.960(46)	9.3787(510)	−0.064 591

s^*	η/mPa s	λ/W m^{-1} K^{-1}	D_{self}/mm s^{-1}
−3.3338	0.388 15(1300)	0.222 94(1200)	$1.8987(163) \times 10^{-5}$
−2.4914	0.175 62(530)	0.173 01(600)	$5.2744(447) \times 10^{-5}$
−1.6576	0.082 168(1700)	0.117 82(860)	$1.3650(96) \times 10^{-4}$
−0.912 27	0.035 334(980)	0.061 351(2000)	$3.6130(305) \times 10^{-4}$
−0.064 591	0.008 186 9(8200)	0.015 338(2200)	$6.6563(388) \times 10^{-3}$

Table S10: Results of propane

ρ/kg/m^3	T/K	p/bar	s^*
721.87	94.076(17)	2.8624(110000)	−4.5467
671.06	143.09(3)	−4.5537(54000)	−3.4475
592.59	220.060(44)	18.218(2700)	−2.3164
432.67	334.470(59)	23.536(1100)	−1.1917
1.1256	220.060(28)	0.461 98(360)	−0.005 494 6

s^*	η/mPa s	λ/W m^{-1} K^{-1}	D_{self}/mm s^{-1}
−4.5467	3.1202(1500)	0.219 45(850)	$1.5769(230) \times 10^{-6}$
−3.4475	0.576 41(2100)	0.181 93(530)	$1.1712(104) \times 10^{-5}$
−2.3164	0.202 68(840)	0.134 54(360)	$4.8891(474) \times 10^{-5}$
−1.1917	0.062 521(1200)	0.076 826(4400)	$1.9923(191) \times 10^{-4}$
−0.005 494 6	0.006 318 9(8300)	0.010 204(1200)	$7.4363(914) \times 10^{-2}$

Table S11: Results of hexane

ρ/kg/m^3	T/K	p/bar	s^*
723.12	207.730(36)	46.542(2100)	−2.7989
668.69	276.560(43)	47.847(1400)	−2.1205
575.01	383.300(84)	50.235(960)	−1.4148
401.83	510.880(55)	48.334(340)	−0.746 57
7.4016	383.300(54)	2.4913(76)	−0.020 003

s^*	η/mPa s	λ/W m^{-1} K^{-1}	D_{self}/mm s^{-1}
−2.7989	0.8528(420)	0.123 25(780)	$1.1487(124) \times 10^{-5}$
−2.1205	0.334 26(2700)	0.112 66(620)	$3.4334(340) \times 10^{-5}$
−1.4148	0.141 19(750)	0.093 022(9600)	$9.8579(909) \times 10^{-5}$
−0.746 57	0.050 907(1200)	0.064 095(5500)	$3.0435(304) \times 10^{-4}$
−0.020 003	0.007 597(600)	0.019 846(2200)	$1.5610(150) \times 10^{-2}$

Table S12: Results of nonane

ρ/kg/m^3	T/K	p/bar	s^*
761.68	219.700(36)	2.0632(28000)	−2.7275
709.08	291.540(48)	8.9105(14000)	−2.0749
616.51	409.07(6)	8.4399(6900)	−1.3849
437.7	563.990(72)	13.847(300)	−0.723 24
2.0972	409.100(52)	0.528 46(260)	−0.005 734

s^*	η/mPa s	λ/W m^{-1} K^{-1}	D_{self}/mm s^{-1}
−2.7275	1.973(110)	0.158 77(1200)	$4.2517(492) \times 10^{-6}$
−2.0749	0.5737(220)	0.132 82(770)	$1.9450(153) \times 10^{-5}$
−1.3849	0.197 07(550)	0.106 63(670)	$6.8291(520) \times 10^{-5}$
−0.723 24	0.062 104(1900)	0.072 336(3700)	$2.4024(168) \times 10^{-4}$
−0.005 734	0.007 307 9(7800)	0.017 784(3800)	$4.5883(674) \times 10^{-2}$

Table S13: Results of 1-butene

ρ/kg/m^3	T/K	p/bar	s^*
799.96	96.575(20)	20.791(2000)	−4.6778
749.86	147.330(25)	1.3977(24000)	−3.5791
669.04	229.440(37)	9.9527(15000)	−2.4138
496	367.170(56)	19.509(610)	−1.2184
0.423 44	229.440(22)	0.140 55(100)	−0.002 004 2

s^*	η/mPa s	λ/W m^{-1} K^{-1}	D_{self}/mm s^{-1}
−4.6778	7.7496(7000)	0.189 84(550)	$6.3405(941) \times 10^{-7}$
−3.5791	0.947 02(4200)	0.176 15(1400)	$7.2819(674) \times 10^{-6}$
−2.4138	0.2834(100)	0.135 18(920)	$3.6013(260) \times 10^{-5}$
−1.2184	0.080 721(2700)	0.076 723(4400)	$1.7151(120) \times 10^{-4}$
−0.002 004 2	0.006 214 3(8600)	0.011 827(3400)	$1.6299(350) \times 10^{-1}$

Table S14: Results of 1-heptene

ρ/kg/m^3	T/K	p/bar	s^*
795.34	169.730(26)	8.0275(25000)	−3.3766
745.48	232.640(39)	11.203(920)	−2.5909
657.97	337.540(46)	9.5989(6700)	−1.7376
476.21	497.05(8)	17.963(400)	−0.890 39
1.1139	337.550(27)	0.307 33(100)	−0.003 625 4

s^*	η/mPa s	λ/W m^{-1} K^{-1}	D_{self}/mm s^{-1}
−3.3766	3.3615(3300)	0.132 87(480)	$2.3048(287) \times 10^{-6}$
−2.5909	0.747 97(4200)	0.123 41(570)	$1.3433(144) \times 10^{-5}$
−1.7376	0.232 09(740)	0.101 67(380)	$5.3644(340) \times 10^{-5}$
−0.890 39	0.071 884(3500)	0.070 874(4500)	$2.1462(188) \times 10^{-4}$
−0.003 625 4	0.007 649(940)	0.015 153(1600)	$7.9637(1088) \times 10^{-2}$

Table S15: Results of dimethylether

ρ/kg/m^3	T/K	p/bar	s^*
851.18	144.840(23)	9.2192(47000)	−3.4617
782.33	202.410(41)	14.712(2600)	−2.6175
670.6	286.67(5)	7.5628(21000)	−1.7364
469.54	389.660(69)	52.462(750)	−0.9114
6.9791	286.670(28)	3.3524(150)	−0.020 621

s^*	η/mPa s	λ/W m^{-1} K^{-1}	D_{self}/mm s^{-1}
−3.4617	1.2459(930)	0.246 26(1100)	$6.2692(747) \times 10^{-6}$
−2.6175	0.3906(200)	0.204 02(870)	$2.5581(237) \times 10^{-5}$
−1.7364	0.152 26(750)	0.140 48(520)	$8.3276(715) \times 10^{-5}$
−0.9114	0.058 587(3000)	0.080 419(5800)	$2.7345(259) \times 10^{-4}$
−0.020 621	0.008 953 3(6500)	0.014 683(1300)	$1.7419(112) \times 10^{-2}$

Table S16: Results of ethanal

ρ/kg/m^3	T/K	p/bar	s^*
867.78	240.500(59)	11.111(4300)	−2.7034
767.93	321.960(58)	2.847(2300)	−2.0673
629.33	412.070(87)	23.247(1800)	−1.4241
424.98	483.030(88)	69.886(590)	−0.827 71
28.14	412.06(5)	17.683(72)	−0.090 534

s^*	η/mPa s	λ/W m^{-1} K^{-1}	D_{self}/mm s^{-1}
−2.7034	0.483 34(1500)	0.251 21(1300)	$2.4264(182) \times 10^{-5}$
−2.0673	0.207 61(490)	0.196 95(1400)	$6.9555(513) \times 10^{-5}$
−1.4241	0.103 72(290)	0.133 34(1100)	$1.6866(132) \times 10^{-4}$
−0.827 71	0.046 199(1400)	0.076 707(4500)	$4.0455(412) \times 10^{-4}$
−0.090 534	0.012 409(1400)	0.023 682(2600)	$5.8509(579) \times 10^{-3}$

Table S17: Results of butanal

ρ/kg/m^3	T/K	p/bar	s^*
887.6	194.480(39)	3.9302(31000)	−3.2082
816.6	270.560(39)	5.4477(18000)	−2.4432
700.87	382.520(79)	5.9733(13000)	−1.6255
491.26	519.630(89)	40.601(630)	−0.852 56
5.1518	382.520(36)	2.1243(65)	−0.014 342

s^*	η/mPa s	λ/W m^{-1} K^{-1}	D_{self}/mm s^{-1}
−3.2082	2.7232(1400)	0.168 09(1500)	$3.4614(314) \times 10^{-6}$
−2.4432	0.565 26(2000)	0.147 87(680)	$1.9936(205) \times 10^{-5}$
−1.6255	0.201 44(1300)	0.113 26(690)	$7.4787(753) \times 10^{-5}$
−0.852 56	0.067 213(4400)	0.085 947(12000)	$2.6619(278) \times 10^{-4}$
−0.014 342	0.010 027(1100)	0.019 798(2100)	$2.4747(231) \times 10^{-2}$

Table S18: Results of heptanal

ρ/kg/m^3	T/K	p/bar	s^*
840.85	252.130(36)	11.371(1500)	−2.5729
776.89	332.03(5)	10.004(1100)	−1.9492
666.84	455.240(69)	9.449(690)	−1.3006
470.79	604.82(8)	30.874(430)	−0.695 29
5.3559	455.220(41)	1.6501(57)	−0.012 129

s^*	η/mPa s	λ/W m^{-1} K^{-1}	D_{self}/mm s^{-1}
−2.5729	1.9113(1200)	0.1404(60)	$5.3695(512) \times 10^{-6}$
−1.9492	0.553 95(4600)	0.128 85(620)	$2.3664(192) \times 10^{-5}$
−1.3006	0.192 92(720)	0.102 34(390)	$8.0727(427) \times 10^{-5}$
−0.695 29	0.064 829(2500)	0.079 916(7100)	$2.6343(194) \times 10^{-4}$
−0.012 129	0.009 236 8(9400)	0.020 528(1700)	$2.2672(221) \times 10^{-2}$

Table S19: Results of acetone

ρ/kg/m^3	T/K	p/bar	s^*
867.62	196.340(36)	3.6394(40000)	−2.877
785.39	279.09(5)	6.8071(28000)	−2.1969
660.67	389.350(57)	9.1299(14000)	−1.4677
458.77	508.55(10)	58.237(540)	−0.800 93
8.7917	389.320(34)	4.4061(80)	−0.025 45

s^*	η/mPa s	λ/W m^{-1} K^{-1}	D_{self}/mm s^{-1}
−2.877	1.5422(570)	0.205 21(1200)	$6.0940(641) \times 10^{-6}$
−2.1969	0.398 05(1400)	0.168 46(950)	$2.9230(228) \times 10^{-5}$
−1.4677	0.154 58(860)	0.118 94(400)	$9.8146(844) \times 10^{-5}$
−0.800 93	0.057 889(2100)	0.072 404(3900)	$3.0273(155) \times 10^{-4}$
−0.025 45	0.010 419(1300)	0.018 319(2100)	$1.4738(103) \times 10^{-2}$

Table S20: Results of butanone

ρ/kg/m^3	T/K	p/bar	s^*
848.2	205.160(42)	8.6126(19000)	−2.8524
775.85	281.70(6)	10.668(2000)	−2.167
657.08	393.700(55)	5.8554(8300)	−1.4307
431.71	527.400(71)	43.736(400)	−0.708 43
6.0661	393.710(44)	2.5430(69)	−0.016 154

s^*	η/mPa s	λ/W m^{-1} K^{-1}	D_{self}/mm s^{-1}
−2.8524	1.7406(810)	0.162 44(1100)	$5.6837(614) \times 10^{-6}$
−2.167	0.454 37(1800)	0.1351(130)	$2.6547(263) \times 10^{-5}$
−1.4307	0.1593(42)	0.102 49(710)	$9.1637(928) \times 10^{-5}$
−0.708 43	0.051 395(1400)	0.066 298(5900)	$3.2439(255) \times 10^{-4}$
−0.016 154	0.009 358 4(7300)	0.017 866(1700)	$2.0597(213) \times 10^{-2}$

Verification of the Nose-Hoover thermostat

We repeated the simulations of hexane with a switched off thermostat in production to check the consistency with the results we obtained with the Nose-Hover thermostat. Figure S1 shows the results for all transport properties in the entropy scaled depiction. The results are equivalent within statistical uncertainties, wether the thermostat is switched on or not.

The results are summarized in table form in Table S21.

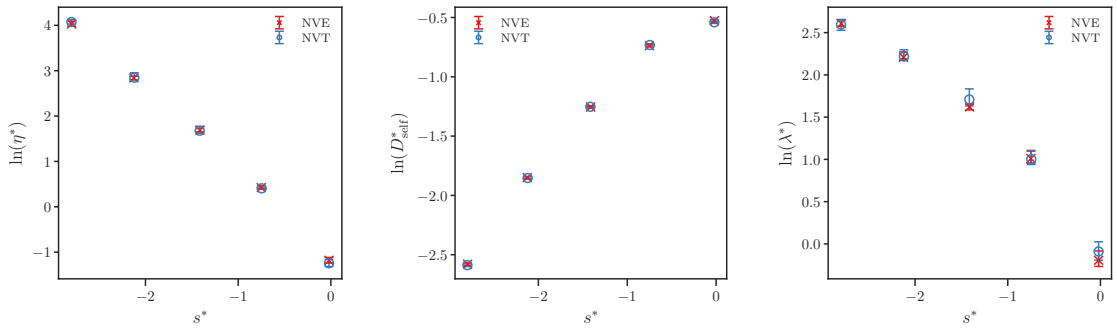

(a) (b) (c)

Figure S1: Logarithmic depiction of reduced viscosity η^* (a), self-diffusion D^*_{self} (b), and thermal conductivity λ^* (c) over residual entropy s^* for hexane. The figure compares the results of simulations with an Nose-Hoover thermostat (NVE) and simulations without any thermostat (NVE)

Table S21: Results of hexane (NVE)

ρ/kg/m^3	T/K	p/bar	s^*
723.12	208.160(66)	52.036(2200)	−2.796
668.69	275.410(35)	36.59(110)	−2.1252
575.01	384.620(17)	56.929(810)	−1.4124
401.83	504.480(29)	38.499(410)	−0.750 66
7.4016	386.47(11)	2.5158(83)	−0.019 807

s^*	η/mPa s	λ/W m^{-1} K^{-1}	D_{self}/mm s^{-1}
−2.796	0.817 81(4600)	0.124 82(500)	$1.1598(126) \times 10^{-5}$
−2.1252	0.331(13)	0.111 18(560)	$3.4336(312) \times 10^{-5}$
−1.4124	0.1433(90)	0.085 467(2900)	$9.8678(711) \times 10^{-5}$
−0.750 66	0.051 185(1700)	0.063 674(4600)	$2.9936(253) \times 10^{-4}$
−0.019 807	0.008 165 1(5100)	0.018 118(1700)	$1.5940(158) \times 10^{-2}$

References

(1) Hemmen, A.; Panagiotopoulos, A. Z.; Gross, J. Grand Canonical Monte Carlo Simulations Guided by an Analytic Equation of State - Transferable Anisotropic Mie Potentials for Ethers. *J. Phys. Chem. B* **2015**, *119*, 7087–7099.

(2) Hemmen, A.; Gross, J. Transferable Anisotropic United-Atom Force Field Based on the Mie Potential for Phase Equilibrium Calculations: n-Alkanes and n-Olefins. *J. Phys. Chem. B* **2015**, *119*, 11695–11707.

(3) Weidler, D.; Gross, J. Transferable Anisotropic United-Atom Force Field Based on the Mie Potential for Phase Equilibria: Aldehydes, Ketones, and Small Cyclic Alkanes. *Ind. Eng. Chem. Res.* **2016**, *55*, 12123–12132.

(4) Dortmund Data Bank, 2018; `http://www.ddbst.com`.

(5) Boushehri, A.; Bzowski, J.; Kestin, J.; Mason, E. A. Equilibrium and Transport Properties of Eleven Polyatomic Gases At Low Density. *J. Phys. Chem. Ref. Data* **1987**, *16*, 445–466.

(6) Mueller, C. R.; Cahill, R. W. Mass Spectrometric Measurement of Diffusion Coefficients. *J. Chem. Phys.* **1964**, *40*, 651–654.

(7) Greiner-Schmid, A.; Wappmann, S.; Has, M.; Lüdemann, H.-D. Self-diffusion in the compressed fluid lower alkanes: Methane, ethane, and propane. *J. Chem. Phys.* **1991**, *94*, 5643–5649.

(8) Helbæk, M.; Hafskjold, B.; Dysthe, D. K.; Sørland, G. H. Self-Diffusion Coefficients of Methane or Ethane Mixtures with Hydrocarbons at High Pressure by NMR. *J. Chem. Eng. Data* **1996**, *41*, 598–603.

(9) Suárez-Iglesias, O.; Medina, I.; de los Ángeles Sanz, M.; Pizarro, C.; Bueno, J. L. Self-

Diffusion in Molecular Fluids and Noble Gases: Available Data. *J. Chem. Eng. Data* **2015**, *60*, 2757–2817.

(10) Panchenkov, G.; Erchenkov, V. Temperature Variation of the Coordination Number and Diffusion Coefficient in a Liquid. *Russ. J. Phys. Chem.* **1962**, *36*, 455–457.

(11) Awan, M.; Dymond, J. Transport Properties of Nonelectrolyte Liquid Mixtures. XI. Mutual Diffusion Coefficients for Toluene + n-Hexane and Toluene + Acetonitrile at Temperatures from 273 to 348 K and at Pressures up to 25 MPa. *Int. J. Thermophys.* **2001**, *22*, 679–700.

(12) D'Agostino, C.; Mantle, M.; Gladden, L.; Moggridge, G. Prediction of Binary Diffusion Coefficients in Non-Ideal Mixtures from NMR Data: Hexane-Nitrobenzene near its Consolute Point. *Chem. Eng. Sci.* **2011**, *66*, 3898–3906.

(13) McCall, D.; Douglass, D.; Anderson, E. Self-Diffusion in Liquids: Paraffin Hydrocarbons. *Phys. Fluids* **1959**, *2*, 87–91.

(14) Harris, K. R. Temperature and density dependence of the self-diffusion coefficient of n-hexane from 223 to 333 K and up to 400 MPa. *J. Chem. Soc., Faraday Trans. 1 F* **1982**, *78*, 2265.

(15) McCall, D. W.; Douglass, D. C.; Anderson, E. W. Diffusion in Liquids. *J. Chem. Phys.* **1959**, *31*, 1555–1557.

(16) Panchenkov, G.; Borisenko, N.; Erchenkov, V. Self-diffusion of n-paraffins in a wide temperature range. *Zh. Fiz. Khim* **1969**, *43*, 2369–2370.

(17) Tofts, P.; Lloyd, D.; Clark, C.; Barker, G.; Parker, G.; McConville, P.; Baldock, C.; Pope, J. Test liquids for quantitative MRI measurements of self-diffusion coefficient in vivo. *Magn. Reson. Med.* **2000**, *43*, 368–374.